BNL-104583-2014-TECH

AGS/AD/Tech Note No. 155;BNL-104583-2014-IR

SEB EMITTANCE MEASUREMENTS

H. Weisberg

October 1979

Collider Accelerator Department

Brookhaven National Laboratory

U.S. Department of Energy

USDOE Office of Science (SC)

DISCLAIMER

Accelerator Department
BROOKHAVEN NATIONAL LABORATORY
Associated Universities, Inc.
Upton, New York 11973

AGS DIVISION TECHNICAL NOTE

No. 155

SEB EMITTANCE MEASUREMENTS

Howard Weisberg
October 17, 1979

SUMMARY

Several details of an analysis of AGS Slow Extracted Beam emittance are discussed. These are: (1) the transport of the extracted beam thru the main magnet fringe field; (2) description of the horizontal beam by r.m.s. emittance parameters; and (3) application of the analysis to the new SEB switchyard.

1. INTRODUCTION

An analysis of SEB emittance has recently been described.[1] In this analysis, measured beam profiles, after appropriate correction, were compared with predictions of a model based on ellipses in vertical phase space and parallelograms in horizontal phase space. Values of the free parameters in the models were obtained. The present report is a supplement to Ref. 1 containing detailed information on several aspects of the analysis that may be useful for future work on AGS extraction and AGS emittance measurement.

2. EXTRACTED BEAM TRANSPORT IN THE MAIN MAGNET FRINGE FIELD

In principle, the emittance of a beam may be measured by observing the variation in beam size as an upstream quadrupole is changed, without any consideration of the beam optics upstream of the quadrupole. When the propagation of systematic errors is considered, however, such measurements may not be accurate. In contrast, the analysis of Ref. 1 uses as much upstream information as possible, in order to reduce the number of free parameters.

In particular the transport matrix from the F5 to the F13 straight sections is used as input, and an accurate value of this matrix is needed.

The matrix is determined by numerical integration in the measured main magnet field, using the "BEAM" computer program.[2,3] For reasonable starting values at F5 and deflection in the F5 and F10 septum magnets, the beam emerges from the fringe field at F13. The beam does not encounter any high-field quadrupoles or sextupoles or backleg windings between F5 and F13. The transport matrix does, however, depend on the initial conditions x, and x' at F5. The initial conditions may be determined by several measured quantities that are listed in Table 1. These include the position of the center of the extracted beam at F5 and F10 (known from septum position readbacks and flag measurements), the deflection of the F10 ejector magnet (known from magnet current measurements) and the beam position outside the machine (known from flag measurements). These data over-determine the orbit.

TABLE 1. Measured quantities at the time of the SEB emittance studies (Feb. 1979).

x (F5)	2.3 in.	(at the center of straight section)
x (F10)	2.1 in.	" " " " " "
$\Delta x'$(F10)	19.1 mrad.	

The beam momentum (at the middle of the momentum sweep) is taken to be 29.0 GeV/c based on previous measurements.[4]

The orbit integration is started at F5 with an assumed position x(F5). The slope x'(F5) is varied to get the correct position x(F10) at F10. The deflection $\Delta x'$(F10) at F10 is then varied to get the correct position outside the machine at the C12 flag.

A number of options are available for the assumed magnetic field, and the sensitivity of the calculated beam transport to these assumptions has been studied. Complete field maps exist at p = 0.308, 12.75 and 33.66 GeV/c, and these are available as field options 1, 2 and 3 in the BEAM program. In addition measurements of the coefficients of a multipole expansion of the integrated field exist at these momenta and at 0.642, 25.68 and 30.83 GeV/c.

In BEAM, the magnetic field for $|x| > 4$ inches is always calculated from the field map. For $|x| < 4$, an option exists either to use the field map or to use the multipole data.

Figure 1 shows the measured multipoles vs momentum. It can be seen that none of three standard field options is a reasonable approximation to the operating field at 29 GeV/c. To try to remedy this shortcoming, BEAM has been modified to enable one to use interpolated multipole values from Fig. 1 so that the field for $|x| < 4$ at least will be realistic. Unfortunately for the fringe field one has to use either the 12.75 GeV/c or the 33.66 GeV/c values.

The best estimate of the transport matrix from F5 to F13 uses the measured values of momentum and position, the interpolated multipole coefficients for 29.0 GeV/c, and the fringe field of field option 2. In addition the matrix has been calculated for variations in these assumptions. The various cases calculated are listed in Table 2. (The best estimate corresponds to Case 3.)

Table 3 shows that the orbit itself is very insensitive to the input assumptions, for the procedure used. Also the F10 septum magnet deflection $\Delta x'(F10)$ comes out to be close to the measured value in Table 1, providing a cross-check of the method.

Table 4 gives calculated values of the horizontal and vertical transport matrices

$$M = \begin{bmatrix} a & b \\ c & d \end{bmatrix} \qquad (1)$$

for the various cases. It is evident that there are significant variations in the calculated values for the different cases. Some of this variation is unimportant, and a better representation of the variation of the calculated values is obtained when the transport matrix is expressed in terms of Twiss parameters as

$$M = \begin{bmatrix} \cos\mu + \alpha \sin\mu & \beta \sin\mu \\ -\gamma \sin\mu & \cos\mu - \alpha \sin\mu \end{bmatrix} \qquad (2)$$

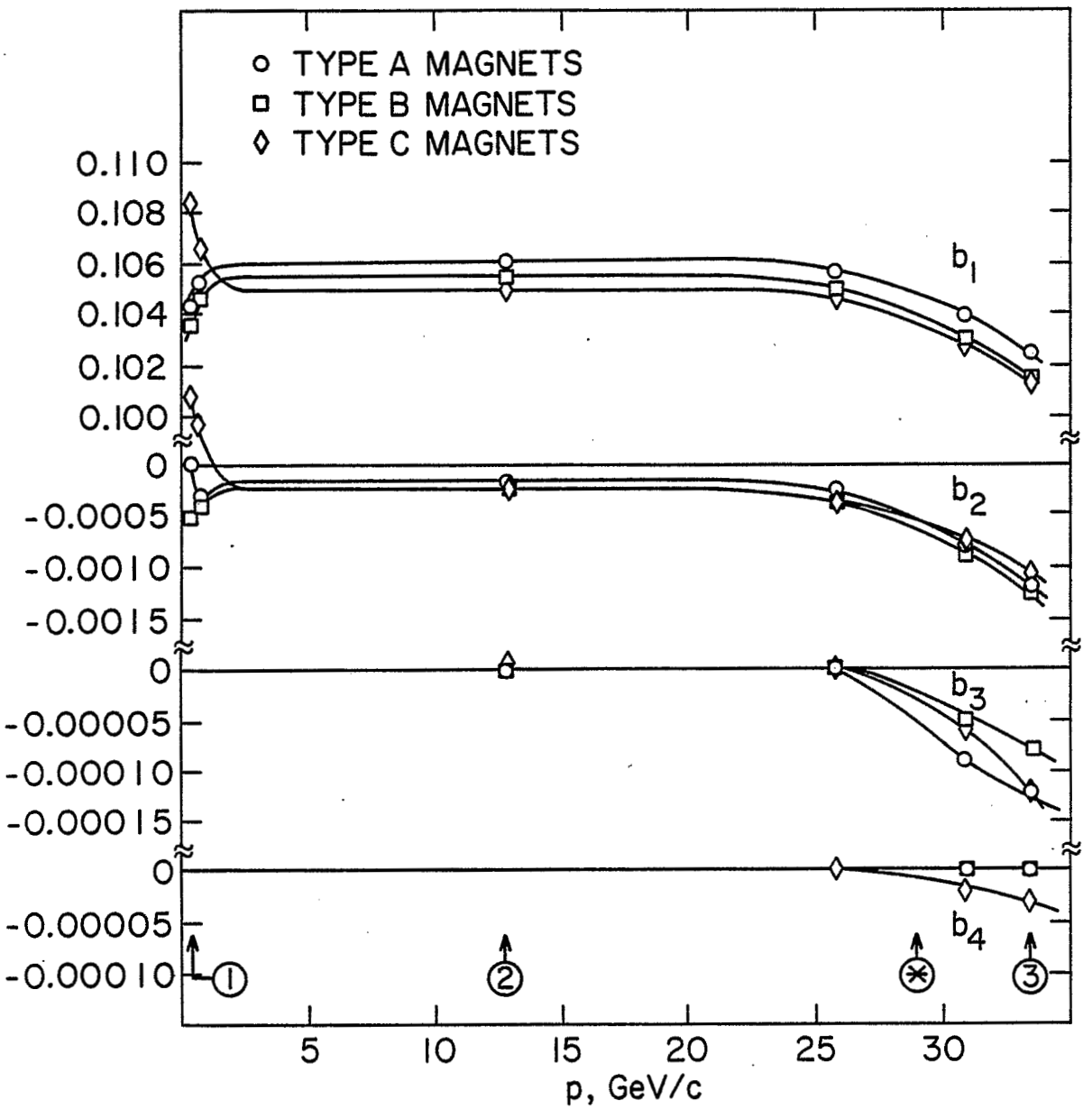

FIGURE 1. Momentum dependence of the multipole moments of the integrated field of the three types of AGS magnets. The field expansion is $B(x) = B_o(1+b_1x+b_2x^2+b_3x^3+b_4x^4)$, with x in inches. Momenta corresponding to field options 1, 2 and 3 and to the normal operating momentum p = 29.0 GeV/c (labeled *) are shown.

TABLE 2. Assumptions for various calculations of the transport matrix from F5 to F13. In Case 2, the multipole expansion for 12.75 GeV/c is used, but the sextupole term b_2 is multipled by 3. Case 3 is considered to be the best estimate. The other cases are calculated to determine the uncertainty in this estimate.

Case	Field Option	Field for $\|x\| < 4$	Momemtum for Multipole Expansion	$\Delta p/p$	x(F5)	x(F10)
1	2	Multipole	12.75 GeV/c	0	2.3 in.	2.1 in.
2	"	"	12.75, $3xb_2$	"	"	"
3	"	"	29.0	"	"	"
4	"	"	"	+1%	"	"
5	"	"	"	0	2.8	"
6	"	"	"	"	2.3	2.6
7	"	Map	———	"	"	2.1
8	"	Multipole	33.38	"	"	"
9	3	"	29.0	"	"	"
10	"	"	33.38	"	"	"
11	"	Map	———	"	"	"

TABLE 3. Beam orbits from F5 to F13 under various assumptions.

Case	x'(F5)	Δx'(F10)	x(F11)	x(F12)	x(F13)	x'(F13)
1	1.77 mr	19.56 mr	4.53 in.	7.50 in.	13.91 in.	56.48 mr
2	1.63	19.26	4.52	7.50	13.91	56.49
3	1.58	19.13	4.53	7.50	13.91	56.49
4	0.94	18.35	4.51	7.48	13.90	56.54
5	1.21	19.85	4.53	7.50	13.91	56.49
6	2.30	17.62	4.77	7.65	14.00	56.11
7	1.70	19.42	4.52	7.50	13.91	56.49
8	1.27	18.74	4.52	7.50	13.91	56.48
9	1.58	19.28	4.53	7.49	13.91	56.51
10	1.27	18.89	4.53	7.50	13.91	56.50
11	1.15	18.62	4.53	7.50	13.91	56.51

TABLE 4. Transport matrices from F5 to F13 under various assumptions. Calculations are for a step size of 1 inch. Units one (inch, mrad) for (x, x').

VERTICAL

CASE	A	B	C	D	IM[MU]	IM[ALPHA]	IM[BETA]	IM[GAMMA]
1	-Ø.257Ø	Ø.2174	-1.7841	-2.3815	-Ø.7792	-1.2345	-Ø.2527	-2.Ø734
2	-Ø.3369	Ø.1918	-1.2239	-2.2717	-Ø.7616	-1.1553	-Ø.2291	-1.4616
3	-Ø.32Ø5	Ø.1869	-1.3925	-2.3Ø79	-Ø.7733	-1.1653	-Ø.2192	-1.633Ø
4	-Ø.3Ø49	Ø.1934	-1.5Ø42	-2.3253	-Ø.7744	-1.1827	-Ø.2264	-1.761Ø
5	-Ø.335Ø	Ø.1841	-1.2681	-2.2883	-Ø.77Ø3	-1.15Ø7	-Ø.2169	-1.494Ø
6	-Ø.34ØØ	Ø.1953	-1.3Ø98	-2.1886	-Ø.7119	-1.1948	-Ø.2525	-1.6932
7	-Ø.3423	Ø.1989	-1.1484	-2.2538	-Ø.7541	-1.1548	-Ø.24Ø3	-1.3875
8	-Ø.3838	Ø.1796	-Ø.8681	-2.1996	-Ø.7463	-1.11Ø5	-Ø.2196	-1.Ø618
9	-Ø.323Ø	Ø.1877	-1.3756	-2.2963	-Ø.768Ø	-1.1666	-Ø.222Ø	-1.6266
1Ø	-Ø.3865	Ø.18Ø3	-Ø.8531	-2.1895	-Ø.7418	-1.11Ø6	-Ø.2221	-1.Ø51Ø
11	-Ø.4912	Ø.1533	-Ø.Ø6Ø9	-2.Ø17Ø	-Ø.6985	-1.ØØ81	-Ø.2Ø25	-Ø.Ø8Ø5

HORIZONTAL

CASE	A	B	C	D	IM[MU]	IM[ALPHA]	IM[BETA]	IM[GAMMA]
1	-Ø.2Ø78	1.2452	-1.551Ø	4.4819	1.3927	1.2415	-Ø.6593	-Ø.8212
2	-Ø.ØØ54	1.3663	-Ø.7517	4.9899	1.5634	1.Ø941	-Ø.5985	-Ø.3293
3	Ø.1ØØ1	1.4458	-Ø.3223	5.3363	1.6574	1.Ø358	-Ø.572Ø	-Ø.1275
4	Ø.1Ø96	1.4427	-Ø.2893	5.3152	1.6551	1.Ø323	-Ø.5722	-Ø.1147
5	Ø.1549	1.4626	-Ø.1112	5.4Ø46	1.6815	1.Ø12Ø	-Ø.5639	-Ø.Ø429
6	Ø.1598	1.4723	-Ø.1ØØ6	5.3314	1.6682	1.Ø113	-Ø.5758	-Ø.Ø393
7	Ø.ØØ93	1.348Ø	-Ø.7Ø79	4.9Ø16	1.5472	1.Ø9Ø8	-Ø.6Ø11	-Ø.3157
8	Ø.4916	1.5879	1.1991	5.9Ø76	1.83Ø8	Ø.891Ø	-Ø.5225	Ø.3945
9	Ø.1Ø46	1.4451	-Ø.3Ø63	5.3296	1.657Ø	1.Ø341	-Ø.572Ø	-Ø.1213
1Ø	Ø.4961	1.5874	1.2151	5.9Ø38	1.83Ø9	Ø.8895	-Ø.5222	Ø.3998
11	Ø.9591	1.7897	3.Ø515	6.7367	2.Ø233	Ø.7775	-Ø.4817	Ø.8212

Therefore calculated Twiss parameters are also given in Table 4 for the transport matrices. This formulation removes some but not all of the variation with input assumptions.

Study of Table 4 yields the following conclusions about the dependence of the calculated transport matrix on input assumptions:

(1) The matrix is stable to variations in assumed momentum, and in position at F5 and F10 (Cases 4, 5 and 6 vs Case 3).

(2) If the multiple expansion for $|x| < 4$ is used, the matrix is insensitive to whether the field option 2 or 3 is used for the fringe field (Case 9 vs Case 3).

(3) The matrix varies significantly when the field for $|x| < 4$ corresponds to magnet excitations other than 29.0 GeV/c. (Cases 1,2,8 vs Case 3).

(4) At fixed magnet excitation there is a significant difference depending on whether the multipole mapped field is used for $|x| < 4$. (Cases 7 vs 1 and 11 vs 10).

Conclusion (4) is the result of an internal inconsistency in either the field measurements or the BEAM program. Until this discrepancy is resolved by further measurements, the amount of difference between Cases 7 and 1 sets the scale of uncertainties in the calculations. We then obtain as best estimates (inch, milliradian units for x and x'):

$$\mu_H = (1.66 \pm 0.15)i \qquad \alpha_H = (1.14 \pm 0.15)i \qquad \beta_H = (0.57 \pm 0.06)i$$

$$\mu_V = \pi - (0.77 \pm 0.06)i \qquad \alpha_V = -(1.17 \pm 0.11)i \qquad \beta_V = -(0.22 \pm 0.03)i \tag{3}$$

Corresponding to these we have

$$M_H = \begin{bmatrix} 0.100 & 1.446 \\ -0.322 & 5.336 \end{bmatrix} \qquad M_V = \begin{bmatrix} -0.321 & 0.187 \\ -1.393 & -2.308 \end{bmatrix} \tag{4}$$

3. PARALLELOGRAM MODEL AND R.M.S. EMITTANCE PARAMETERS

3.1 Vertical Plane

In the analysis of Ref. 1, the vertical beam is described by Gaussian ellipses in phase space. The parameter of the model which was fit to the measurements is the r.m.s. emittance $E_y^{r.m.s.}$. To complete the description of the beam in this model one has the Twiss parameters of the AGS lattice at F5, which are known. Using the vertical transport matrix from F5 to F13, one may then calculate Twiss parameters at the standard reference point F13, which is then taken as the origin of the SEB for calculation of beam size for example by the TRANSPORT or EMITT computer programs. In addition we scale up the emittance by

$$E_y^{99\%} = -\,2\,\ell n\,(.01)\,E_y^{rms} = 9.21\,E_y^{rms} \quad . \tag{5}$$

The beam envelopes thus calculated will contain 99% of the particles in phase space, and 99.76% of the particles at a given location. They provide a conservative basis for the choice of apertures in the beam transport system.

3.2 Parallelogram Model of Horizontal Plane

The horizontal beam is described by a parallelogram model, which does not lend itself so directly to beam envelope calculation by standard methods. In analogy to the vertical beam, we have the measured parameter Δ, and the remaining parallelogram parameters at F5 r, s and t, as described in Ref. 1. If we take

$$\Delta^{99\%} = \sqrt{-2\ell n(.01)}\;\Delta = 3.035\;\Delta = (0.21 \pm 0.06)\ \text{mrad} \tag{6}$$

we obtain a parallelogram at F5 containing 99% of the particles in phase space.

The measurements of Ref. 1 were made without the H20 electrostatic septum in operation, and the beam had spiral pitch r = 0.8 in. Subsequent operation, and planned future operation with the new switchyard, is with reduced spiral pitch r = 0.6 in. The parallelogram area with r = 0.6 is then

$$E_x^{99\%}\ (\text{parallelogram model}) = r\cdot\Delta^{99\%} = 0.040\pi\ \text{in-mrad} \quad . \tag{7}$$

This parallelogram may be transported to any downstream point. Its projection then gives a beam envelope containing 99% of the particles in phase space, in the parallelogram model. Further properties of the beam, such as profile shapes, may be determined by Monte-Carlo ray tracing techniques as in Ref. 1, starting from the postulated phase space distribution at F5.

The phase space coordinates of the corners of the model parallelogram at the F13 reference point are given in Table 5.

3.3 R.M.S. Emittance Model of Horizontal Plane

In some cases it will be convenient to have an approximate description of the horizontal beam along more conventional lines, and this may be provided by the method of r.m.s. emittances.[5]

Let $\rho(x,x',s)$ describe the distribution in phase space of an arbitrary beam which propagates along s in a linear beam transport system; ρ is normalized so that $\int \rho(x,x')dxdx' = 1$. Define second moments of the beam by

$$M_{\mu\nu} = \int (x-\bar{x})^{\mu} \, (x'-\bar{x'})^{\nu} \, \rho(x,x') \, dx \, dx' \tag{8}$$

where $\bar{x}$ and $\bar{x'}$ are the first moments given by

$$\begin{aligned} \bar{x} &= \int x \, \rho(x,x') \, dx \, dx' \\ \bar{x'} &= \int x' \, \rho(x,x') \, dx \, dx' \quad . \end{aligned} \tag{9}$$

Then the r.m.s. emittance E_{rms} is defined by

$$E_{rms}/\pi = \varepsilon_{rms} = \left[M_{20} \, M_{02} - (M_{11})^2 \right]^{\frac{1}{2}} \tag{10}$$

and r.m.s. Twiss parameters are defined by

$$\begin{aligned} \beta_{rms} &= M_{20}/\varepsilon_{rms} \\ \alpha_{rms} &= -M_{11}/\varepsilon_{rms} \\ \gamma_{rms} &= M_{02}/\varepsilon_{rms} = (1 + \alpha_{rms}^2)/\beta_{rms}. \end{aligned} \tag{11}$$

With these definitions ε_{rms} is invariant and $\beta_{rms}, \alpha_{rms}, \gamma_{rms}$ transform with s by the usual transformations for Twiss parameters. These parameters then provide a representation of an arbitrary beam by an ellipse in phase space. This representation, although only approximate in general, provides an exact description of the second moments of the beam, including the r.m.s. width $\sigma = \sqrt{M_{20}}$ which may be determined from measured beam profiles.

R.M.S. emittance parameters have been calculated for the SEB by Monte-Carlo ray tracing. The results, at the F13 reference point, are given in Table 6. The horizontal emittance corresponding to 99% of the particles in phase space has been obtained from the r.m.s. emittance of Eq. 10 by means of Eq. 5, although Eq. 5 is valid only for a beam with Gaussian profiles. The result,

$$E_x^{99\%} \text{ (r.m.s. approximation)} = 0.072\ \pi \text{ in-mrad} \qquad (12)$$

differs significantly from the (presumably more reliable) result for the parallelogram model given in Eq. 7.

Table 6 also contains the r.m.s. parameters for the vertical plane as discussed above in Section 3.1.

4. IMPLICATIONS FOR THE NEW SEB SWITCHYARD

4.1 Beam Envelopes

The parameters of Table 6 are substantially the same as those assumed in the design of the new SEB switchyard.[6] Studies have shown that solutions can be found for the matching quadrupoles CQ_{1-4} for these and similar parameters. Table 7 gives quadrupole settings for three cases. Case 1 is for the assumptions of the design report, Ref. 6. Case 2 is for the emittance parameters determined in this study and given in Table 6; the quadrupoles are set to provide the same output β and α as in the design report. Case 3 is discussed below.

Figures 2-4 show the calculated beam envelopes in the A, B/C and D lines for the assumed input parameters of Table 6 and the quadrupole settings of Table 7, Case 2. In these figures the solid lines marked V gives the vertical

TABLE 5. Coordinates in horizontal phase space of vertices of the model SEB parallelogram at the middle of the F13 straight section.

Vertex	x, in.	x', mrad
1	-0.304	0.724
2	-0.159	0.587
3	0.304	-0.724
4	0.159	-0.587

TABLE 6. SEB emittance parameters at the F13 reference point. The horizontal values are obtained from parallelogram model calculations by the method of r.m.s. emittances, using Eq. 5 to obtain $E^{99\%}$.

Plane	Horizontal	Vertical
$E^{99\%}$	0.072 π	0.087 π in-mrad
β	2.30	0.130 in-mrad^{-1}
α	-6.6	0.87

TABLE 7. Parameter values for three different settings of the matching quadrupoles CQ_{1-4}, as discussed in the text.

			Datacon Settings		
Quadrupole	Effective Length, in.	Gradient Constant, kG/in/Datacon Count	Case 1	Case 2	Case 3
CQ_1	37.5	0.00347	1199	1533	1867
CQ_2	49.5	-0.00463	1370	1378	1155
CQ_3	49.5	0.00463	1516	1195	466
CQ_4	37.5	-0.00347	1605	1299	717

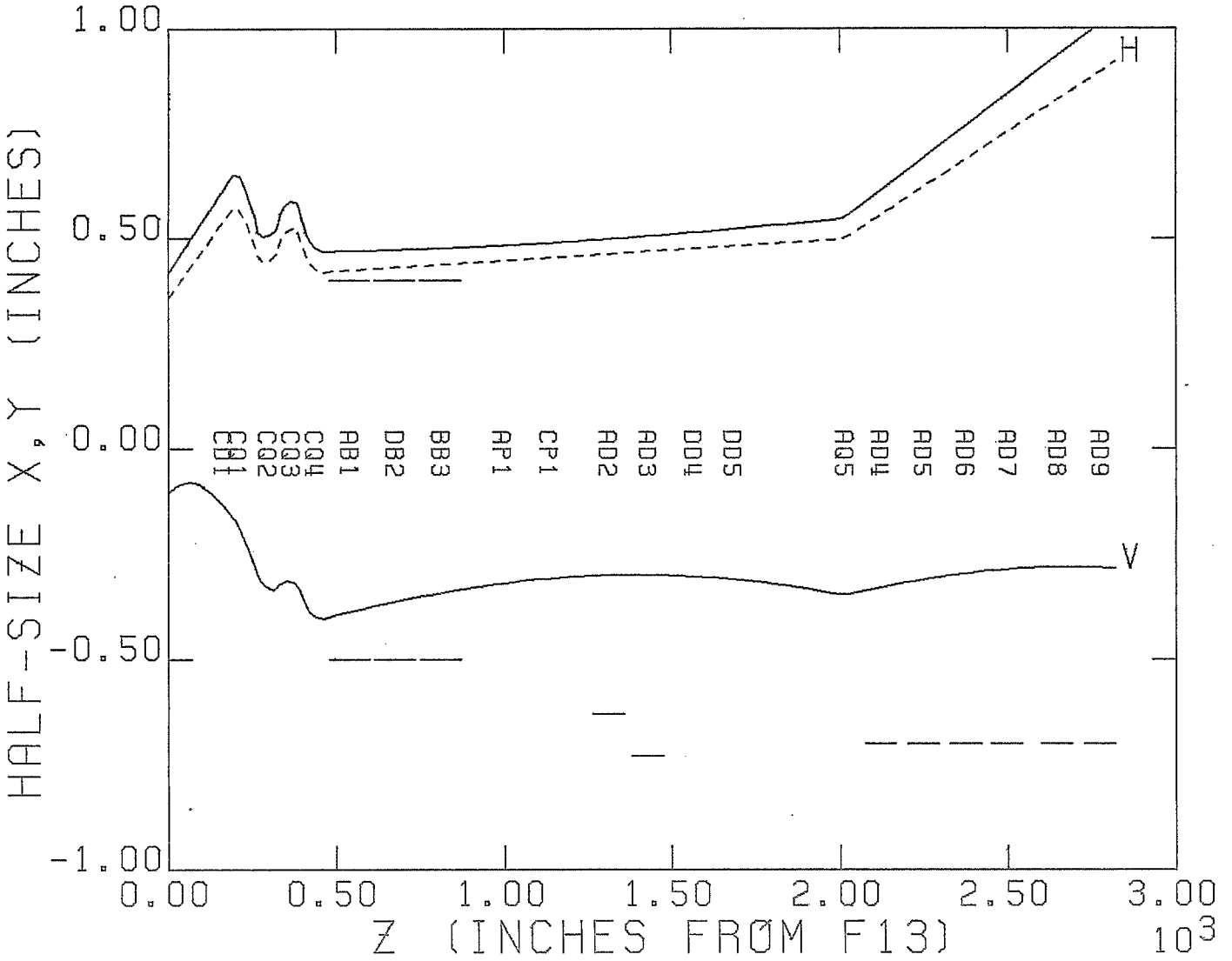

FIGURE 2. Predicted beam prifiles in the A line.

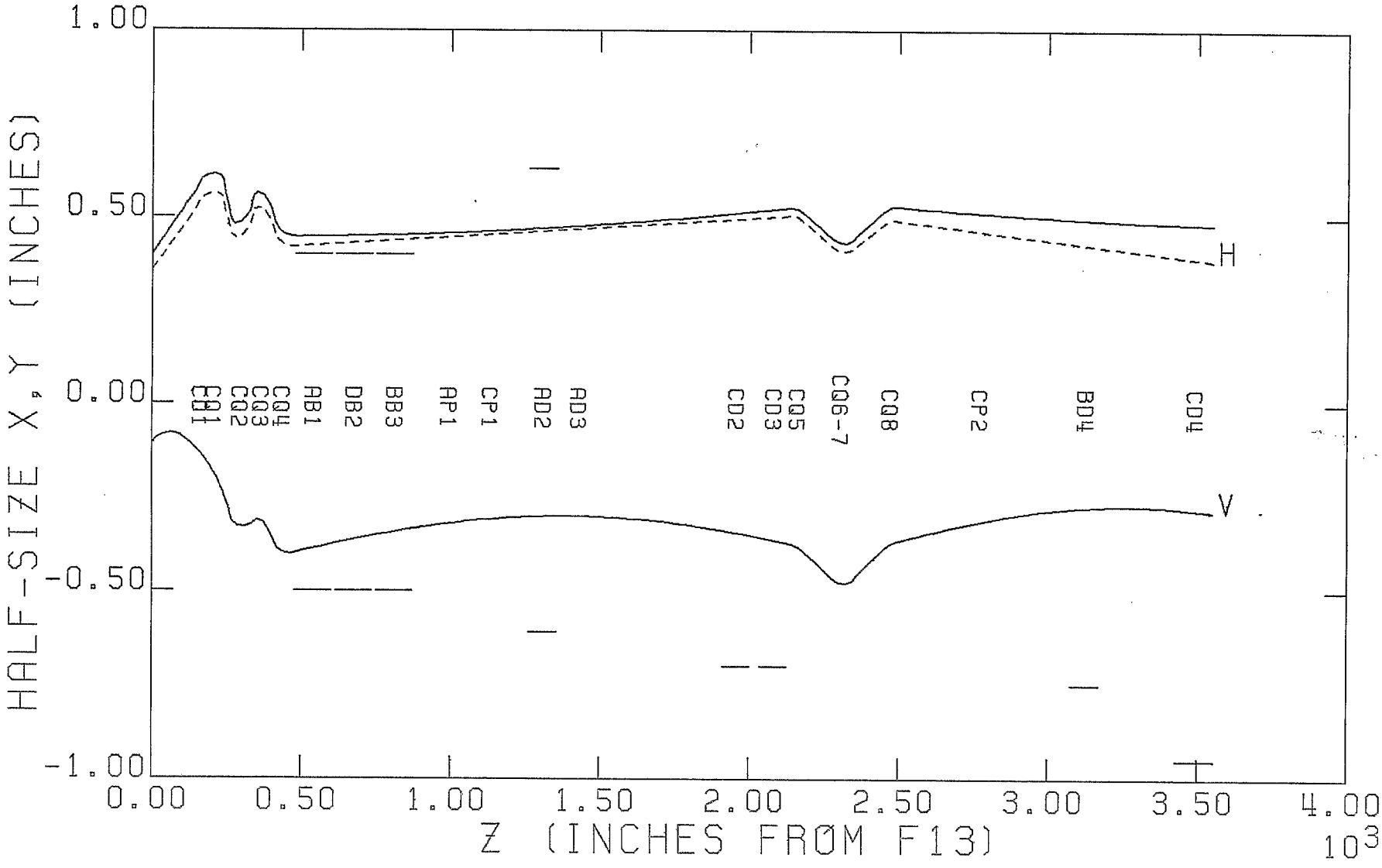

FIGURE 3. Predicted beam prifoles in the B and C lines.

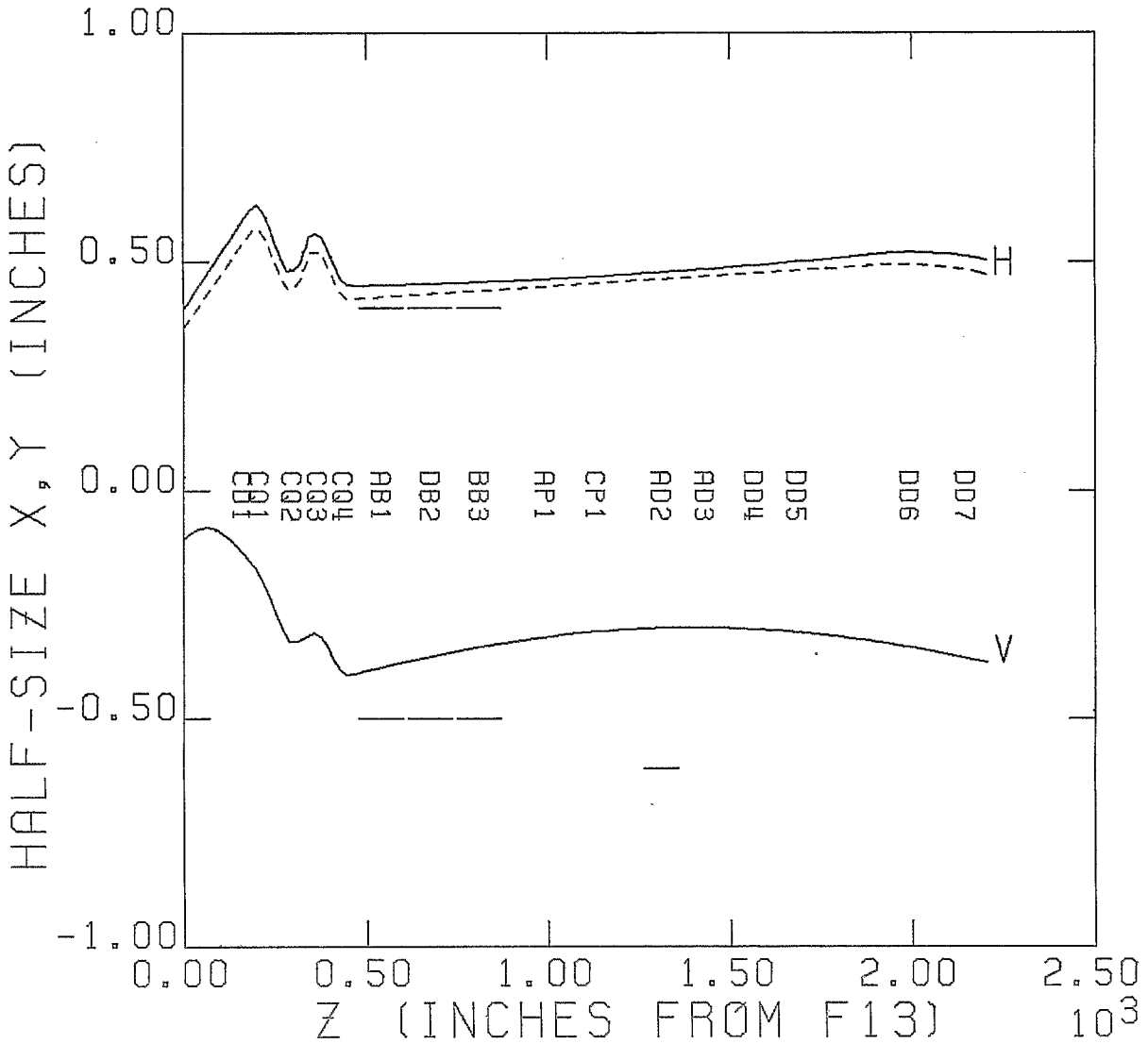

FIGURE 4. Predicted beam profiles in the D line.

envelope, the dashed line marked H gives the horizontal envelope in the parallelogram model, and the remaining solid line gives the horizontal envelope in ellipse approximation using r.m.s. parameters as discussed above. The horizontal envelopes in the ellipse and parallelogram models are substantially similar. Comparison with the corresponding plots in Ref. 6 shows that the envelopes in Figs. 2-4 are also substantially the same as these obtained with design report parameters.

Also shown on Figs. 2-4 are some of the critical apertures that the beam has to pass thru without scraping. The beams in general are smaller than the apertures with enough room to allow for misalignments and instabilities. However, the horizontal beam at the electrostatic beam splitters AB1-BB3 is somewhat larger than the 0.4 inch half size that corresponds to the distance from the wire septum to a cathode. Normally some beam is desired on both sides of the septum, but in cases that call for almost 100% of the beam to be on one side of a septum, there would be some beam scraping on the cathode on that side. Therefore, for these cases a different quadrupole tune is needed. Such tunes can easily be achieved, as indicated in Fig. 5 which corresponds to the tune quadrupole settings in Case 3 of Table 7.

Figures 6-8 show predictions for the outline in phase space containing 99% of the beam for the horizontal beam in both the parallelogram model and the ellipse approximation, and for the vertical beam. Also shown are predicted beam profiles obtained by projecting the phase space distribution on the horizontal axis.

An interactive computer program called CQTUNE is being developed for the AGS control computer to control the matching quadrupoles CQ1-4 operationally to obtain optimum values for various switchyard conditions.

4.2 Septum Losses

One may want to run with the larger beam of Case 2 where possible, because it corresponds to lower septum losses than does Case 3. The beam loss on an electostatic septum is given by

$$L = w\ (t_1 + t_2 + t_3) \quad . \tag{13}$$

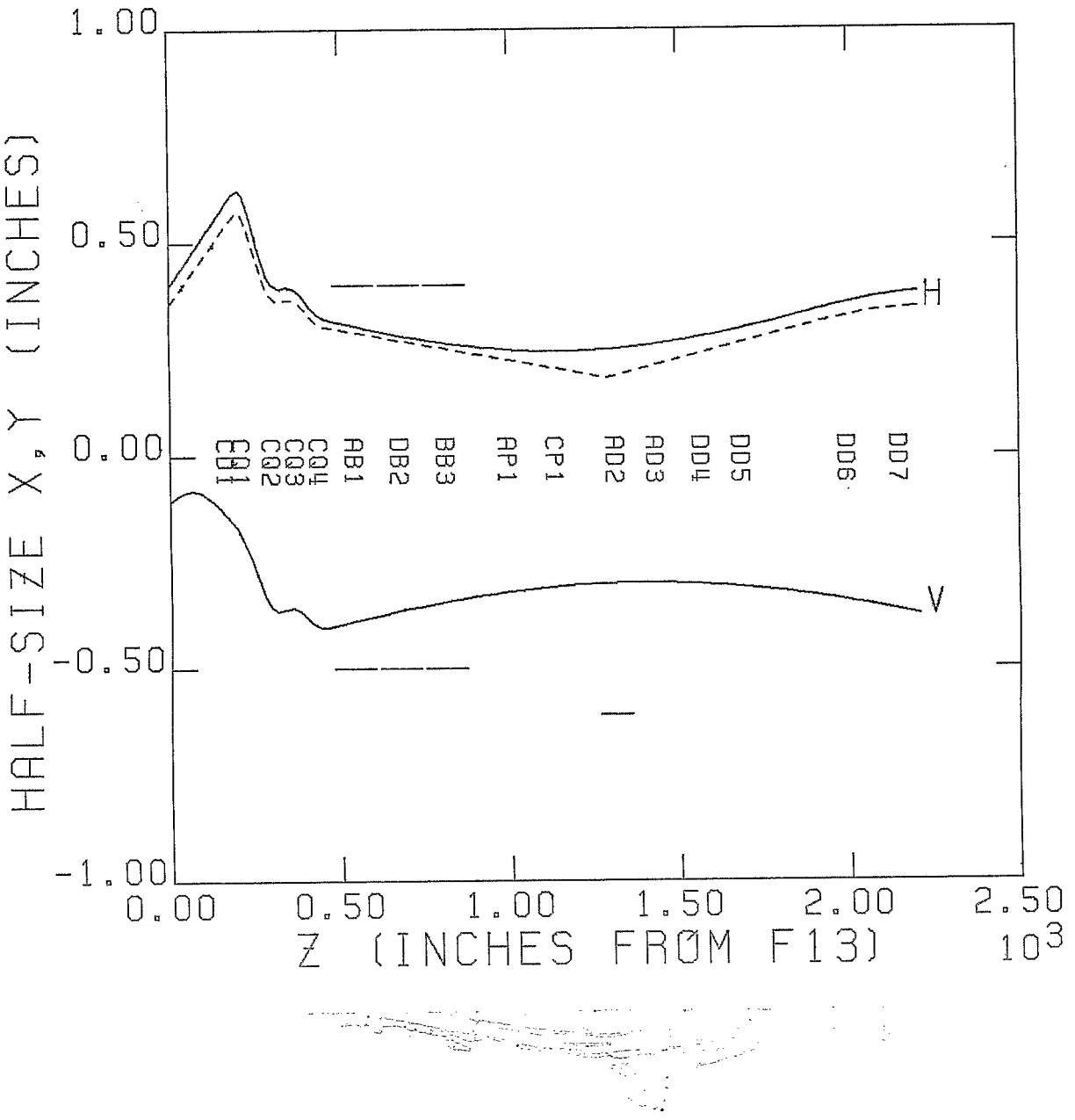

FIGURE 5. Predicted beam profiles with matching quads readjusted for minimum beam size in the electrostatic splitters.

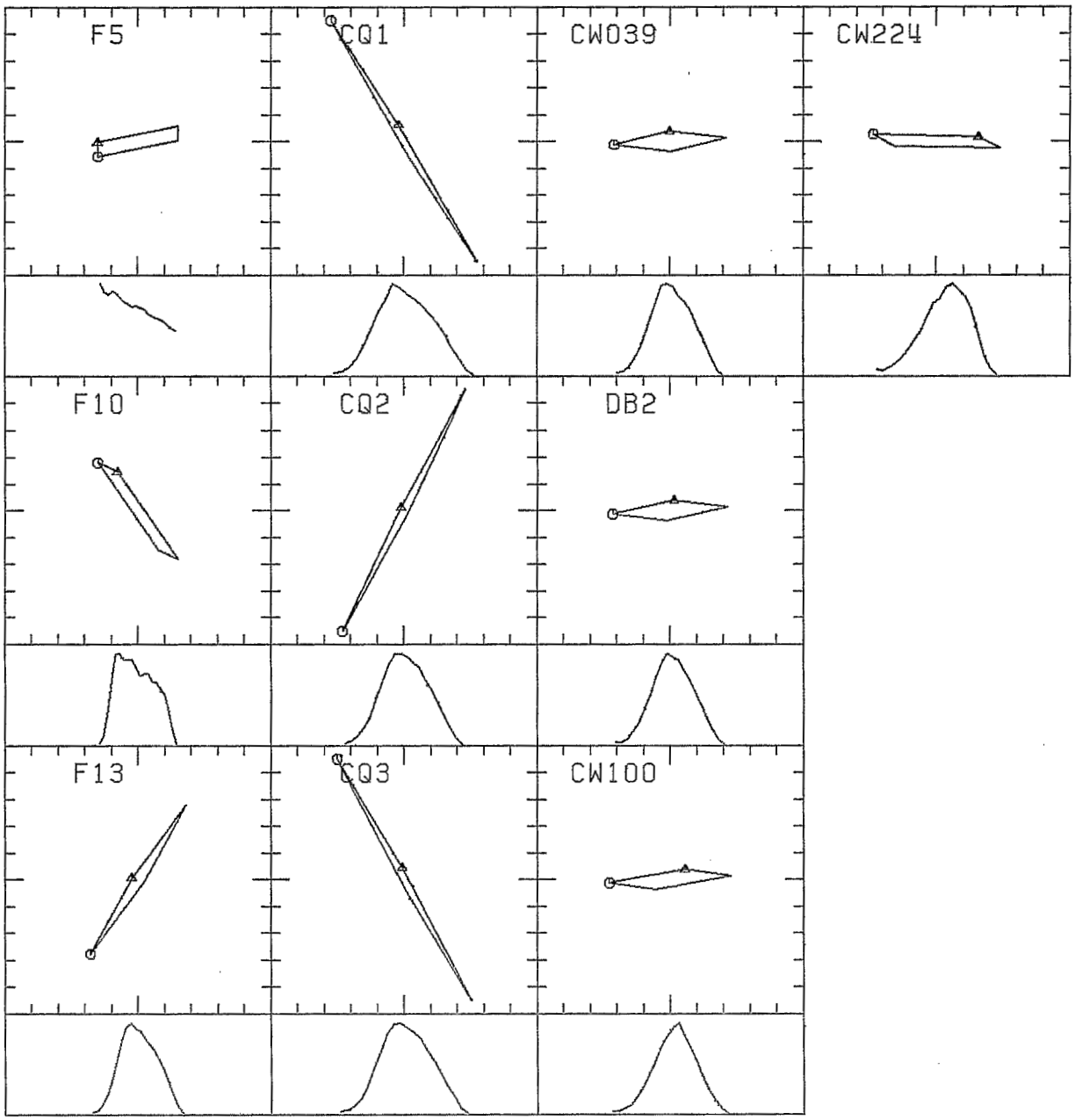

FIGURE 6. Predicted beam distributions in horizontal phase space and corresponding beam profiles obtained by Monte Carlo ray tracing in the parallelogram model. The range of the plots is ± 1 inch in x and ± 2 mrad in x'.

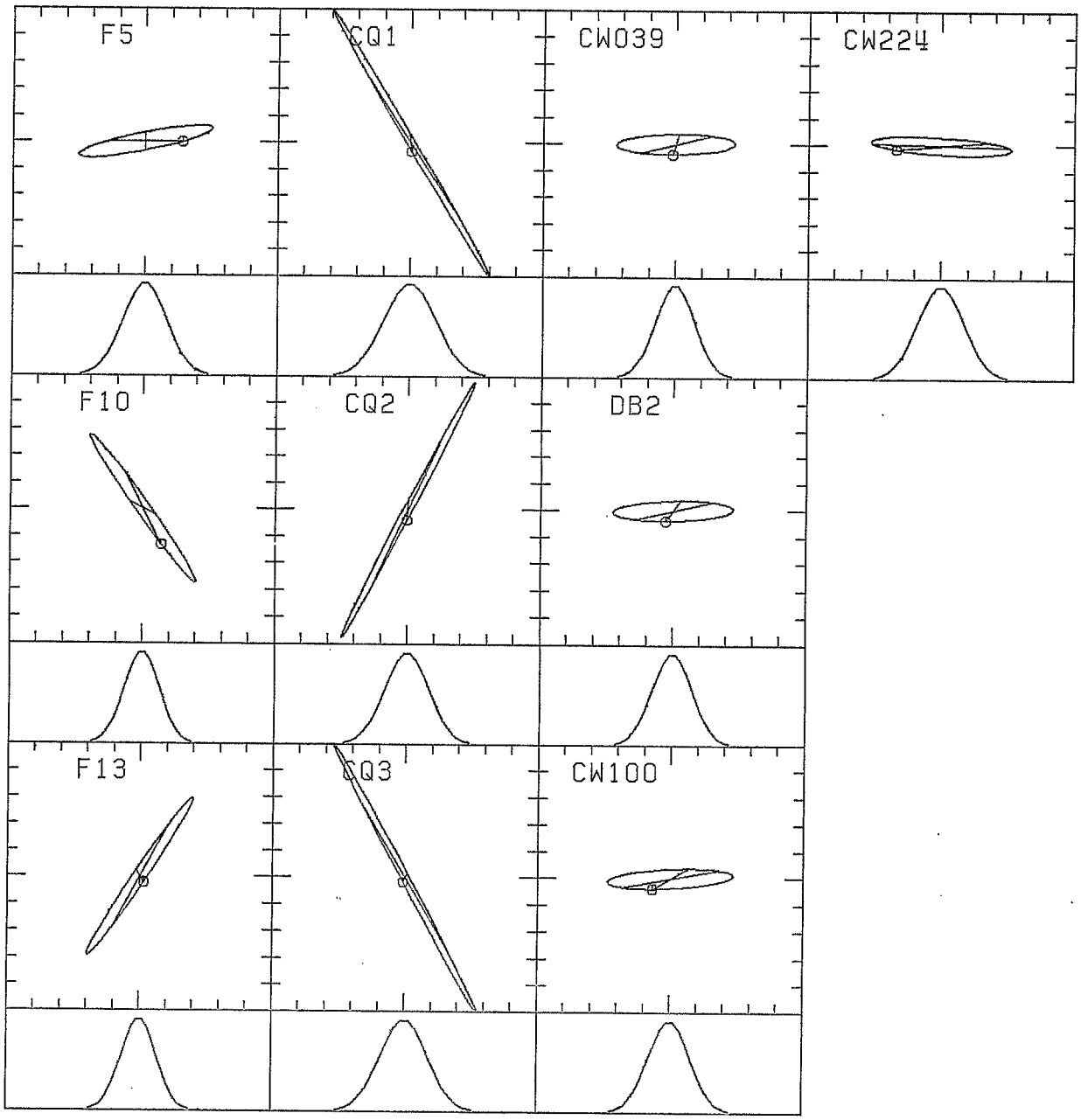

FIGURE 7. Predicted beam distributions in horizontal phase space and corresponding beam profiles for a Gaussian ellipse approximation to the beam obtained by the method of r.m.s. emittances. The range of the plots is ± 1 inch in x and ± 2 mrad in x'.

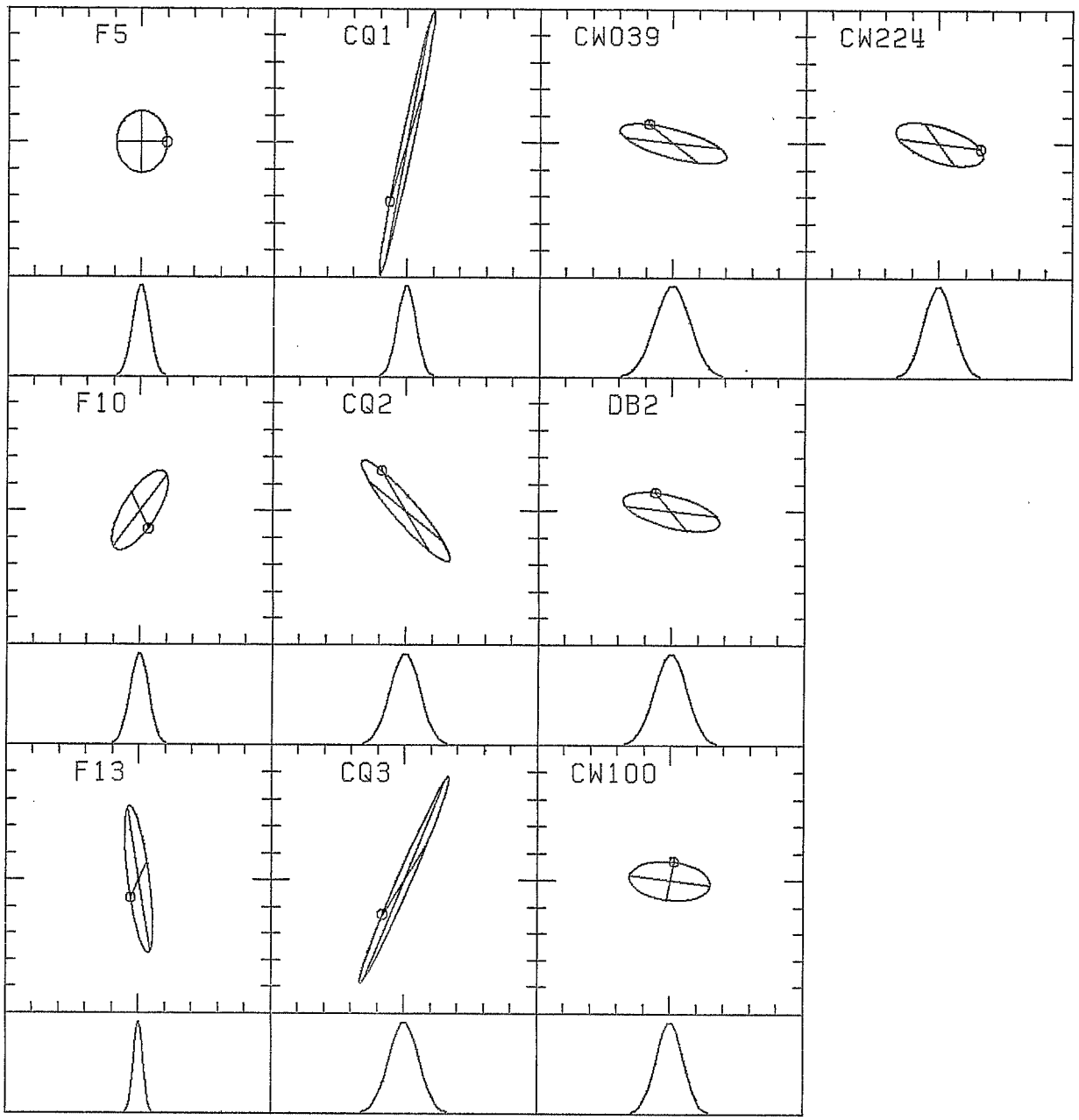

FIGURE 8. Predicted beam distributions in vertical phase space and corresponding beam profiles for a Gaussian ellipse model. The range of the plots is ± 1 inch in y and ± 2 mrad in y'.

where w is the beam density distribution (equal to the inverse of the beam size for a uniform beam density); t_1 is the septum wire diameter; t_2 is an allowance for construction tolerances; and t_3 is the contribution to septum effective thickness due to beam divergence. The contribution t_3 is given in turn by

$$t_3 = \frac{1}{2} \rho \, \theta_{rms}^2 \qquad (14)$$

where $\rho = pc/e\mathcal{E}$ is the radius of curvature of a beam particle of charge e and momentum p in an electric field $\mathcal{E}$ and θ_{rms} is the r.m.s. beam divergence. When the beam is made smaller, both w and θ_{rms} increase. Relevant numerical values are given in Table 8.

According to calculation, there should be no significant beam loss at the thin Lambertson septa for either tune. This is illustrated for the example of the first thin Lambertson AP1 in Table 9. The clearances at the other thin Lambertson's CP1 and CP2 are similar.

REFERENCES

1. H. Weisberg, "Improved Measurements of Slow-Extracted Beam Emittance," BNL-26492 and Nuclear Instruments and Methods, to be published.
2. E.D. Courant, "Computations of AGS Orbits with 704 Computer," Accelerator Department Report EDC-36 (1960).
3. G.H. Morgan, "The Fortran IV Version of BEAM, the AGS Orbit Computing Program," Accelerator Department Report GHM-1 (1966).
4. H. Weisberg, "Gauss Clock Calibration", AGS Tech Note 145 (1978).
5. H. Brown, notes.
6. L. Blumberg, H. Brown, et al., "Design of the New Slow External Beam Switchyard," BNL 24508.

/lsk

Distr: Dept. Admin.

TABLE 8. Quantities related to electrostatic septum beam loss in the new SEB switchyard. Parameters used are t_1 = 0.002 in., t_2 = 0.001 in., pc/e = 29 GeV, and ε = 34 kV/cm. Cases 2 and 3 correspond to matching quad settings that give different beam sizes in the electrostatic splitters. The values of w are given at the peak of the beam density distribution. The loss L is for a single septum.

Case	2	3
w, in^{-1}	2.4	3.9
θ_{rms}, μrad	51	87
t_3, in.	0.00044	0.00126
L, percent	0.8	1.7

TABLE 9. Beam clearance at thin Lambertson septum AP1. Values are for pc/e = 29 GeV, $\mathcal{E}$ = 34 kV/cm, distance from AB1 center to AP1 upstream end = 393 in., AP1 septum thickness = 0.030 in. Beam divergence is for the parallelogram containing 99% of the beam.

Case	2	3
AB 1 Septum Deflection, mrad	0.72	0.72
Total Beam Divergence, mrad	0.30	0.41
AP 1 Septum Clearance, in.	0.135	0.092